Nancy Grace Roman Space Telescope (Roman) Technical Report

Title: Characterizing and Correcting the Anomalous First Read of Detector 18 on Roman-WFI	Doc #: Roman-STScI-000867 Date: 11 November 2025 Rev: -
Author: Timothy D. Brandt	Release Date: 25 November 2025

ABSTRACT

The first read of WFI18, one of the eighteen detectors of the Roman Wide Field Instrument (WFI), has a transient signal in the first read with an amplitude as high as ≈100 DN. If not corrected, this transient would render the first read unusable for science data for much of the detector. This Technical Report characterizes the transient signal in WFI18, proposes a functional form that fits the signal well, and proposes an algorithm to remove the transient during data processing before fitting each pixel's count rate. The first read transient is strongly temperature dependent, with significant exposure-to-exposure variations also observed in thermal vacuum testing of Roman-WFI. A static correction is therefore inadequate: the first read transient must be fit separately in every exposure.

Operated by the Association of Universities for Research in Astronomy, Inc., for the National Aeronautics and Space Administration under Contract #80GSFC19C0054

1 Introduction

Exposures taken using the Wide Field Instrument on the Roman Space Telescope (Roman-WFI, Domber et al. 2022; Schlieder et al. 2024) are taken in a nondestructive readout mode. Many individual reads are taken, with some optionally averaged together into resultants on board the spacecraft. The resultants are then sent back to Earth where they can be used to fit for the count rate of each pixel. These count rate images form the basis of further scientific analysis.

An ideal detector would linearly accumulate signal starting from a (possibly unknown) reset value. Real detectors have various forms of nonideal behavior, including nonlinearity, interpixel capacitance, the brighter-fatter effect, and persistence. This document quantifies a different nonideal effect: an anomalous, large-amplitude transient signal in the detector WFI18 on Roman-WFI. The transient behavior in question is primarily, but not entirely, confined to the first read. The first read is particularly valuable when fitting a count rate to each pixel: it extends the integration time and provides dynamic range for pixels that saturate later in the ramp. Removing this transient is necessary to enable the full use of the first read of WFI18 for science operations.

The pixels on each detector of Roman-WFI are reset in order, one pixel at a time. Immediately after being reset, each pixel is read out; this is sometimes termed the *reset read*. There are 4096×4096 pixels on each detector, the pixel reset and read rates are both 200 kHz, and there are additional delays at the end of reading each row and when reading out guide windows during an exposure. It thus takes several seconds for all pixels on the detector to be reset and read out. After all pixels have been read, the electronics return to the first pixel and the next readout cycle begins. The reset read exhibits anomalies from the signal expected from a constant accumulation of signal. These anomalies, their temporal stability, and their dependence on illumination, will be the subject of a future investigation. This report is concerned with the first regular science read. For a given pixel, this first regular read occurs several seconds after reset.

2 The Anomalous First Read

In this section we will quantify the deviation of the first read of WFI18 from ideal detector behavior. For an ideal detector, the first read would have the signal expected from fitting a constant count rate to later reads and extrapolating back. We will consider the residuals of the first read from this extrapolation. We visualize these residuals using a 55-read unilluminated exposure from TVAC2, the second round of thermal-vacuum (TVAC) testing of Roman-WFI. By using an unilluminated exposure, we avoid the complication of having to correct for nonlinearity. We first remove correlated $1/f$ noise (Rauscher et al. 2007; Rauscher 2015) using the Improved Roman Reference Correction (IRRC, Betti et al. 2024). We then fit a linear accumulation of signal to Reads 3-55 of the exposure,

$$\text{signal} = \text{reset} + \text{rate} \times \text{time}. \tag{1}$$

This gives a predicted signal level in the first read. The difference between the measured signal level and this predicted signal level is what we will term the *first read residual*.

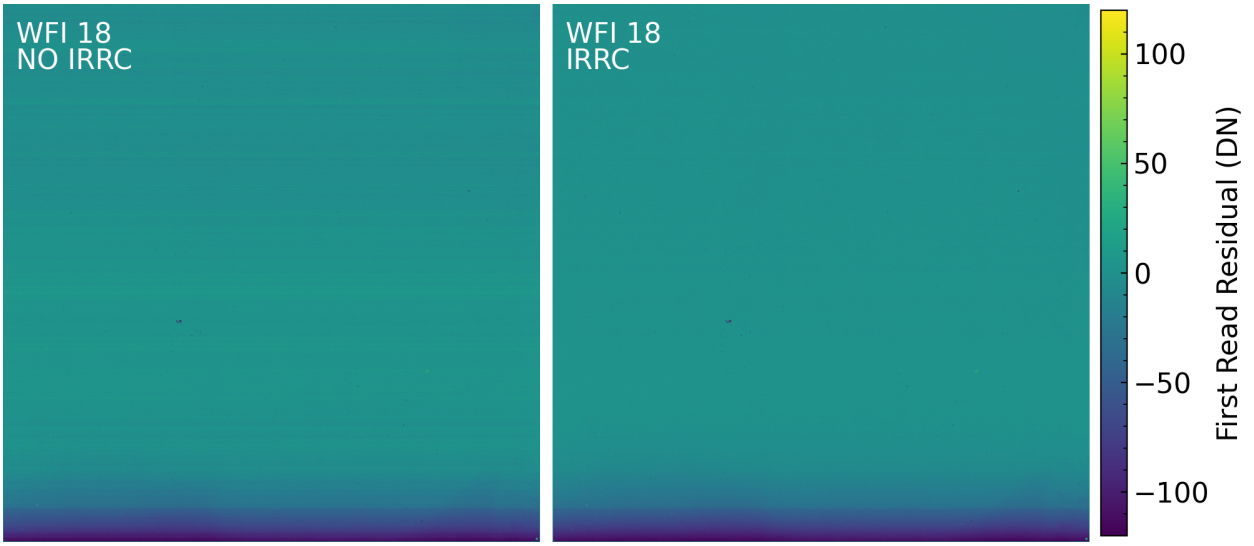

Figure 1: Residual of the first read of an unilluminated ramp of the detector WFI18 from a constant accumulation fit to reads 3-55 and extrapolated back to the first read. There is a visible transient with a peak value of ≈−100 DN at the bottom of the detector (where the readout begins). The left panel shows the data without the improved Roman reference correction (IRRC); significant $1/f$ noise is visible. The remainder of this Technical Report will use data that has been processed with the IRRC.

Figure 1 shows the first read residual for a single exposure. The left panel shows the residual as derived without any use of the reference pixels, while the right panel shows the residual after processing the data using the IRRC. Without the IRRC, there is $1/f$ noise clearly visible. These stripes are strongly correlated along rows, making it much more difficult to use row averaging to increase the signal-to-noise ratio.

The first read residual has a large negative value of ≈100 DN at the edge of the detector that is read out first. This residual is especially clear on the IRRC-corrected frame. While the detector is read out simultaneously in 32 readout channels, these channels are not visible in the figure, and the average values of the residual in each channel do not show measurable differences. This suggests that the first read residual is independent of readout channel. For subsequent analyses, we therefore average the channels together.

The pixels in the Roman-WFI detectors are read out in order, where the readout proceeds horizontally across a row, and then continues to the next row after the previous row has been read out. Readout is fast along rows and slow along columns. To simplify the analysis here, we use sigma-clipped averaging to characterize the first read residual with a single number per row per exposure. This neglects the small, but known, difference in read times between different pixels in the same row (these differences can be fully accounted for when applying a correction). Our use of row averaging makes the use of the IRRC to obtain high signal-to-noise ratio results.

Figure 2 shows the data from Figure 1 but with a single measurement per row. The first four points near zero are rows of reference pixels that do not share the anomaly seen in the science pixels. Two other features are clearly visible. First, there is a gap at Row 256 and, though less visibly, at other multiples of 256 rows. This is due to a pause in reading out

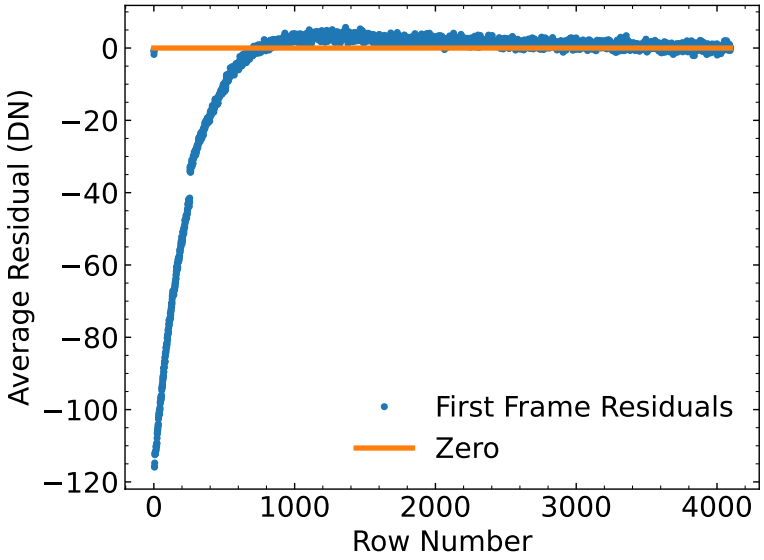

Figure 2: The same data as that shown in Figure 1, with a sigma-clipped mean over columns for each row. Discontinuities are visible every 256 rows. These are due to intervals where readout of science pixels is paused while the guide window is being read out. The orange line shows zero for reference. The first four rows are reference pixels and do not show the anomalous behavior seen in the science pixels.

science pixels as the detector reads out guide window pixels instead. Second, the transient begins as a large, negative offset, but crosses zero before decreasing towards the end of the first read.

3 A Functional Form for the Residual

Knowing the full pixel timing pattern, including the time gap required to read out the guide window, we can transform the horizontal axis of Figure 2 into time. We can then attempt to find a functional form that describes the anomalous behavior seen in the first read. An exponential provides a good fit to the behavior in the initial rows, but it cannot match the positive residuals seen later in the first read. We therefore fit the sum of two exponentials, each with their own coefficient and time constant:

$$\text{residual} = a \exp\left[-t/\tau_a\right] + b \exp\left[-t/\tau_b\right]. \tag{2}$$

Figure 3 shows the best-fit double exponential given by Equation (2). The best-fit single exponential is also shown for comparison as a dashed black line. The double exponential provides a much better fit, particularly at early and at late times. The lower panels of Figure 3 show the residuals from Equation (2). While there may be a systematics as large as ∼1 DN in pixels read out immediately after returning from reading the guide window, the residuals are typically <1 DN and appear to be mostly random.

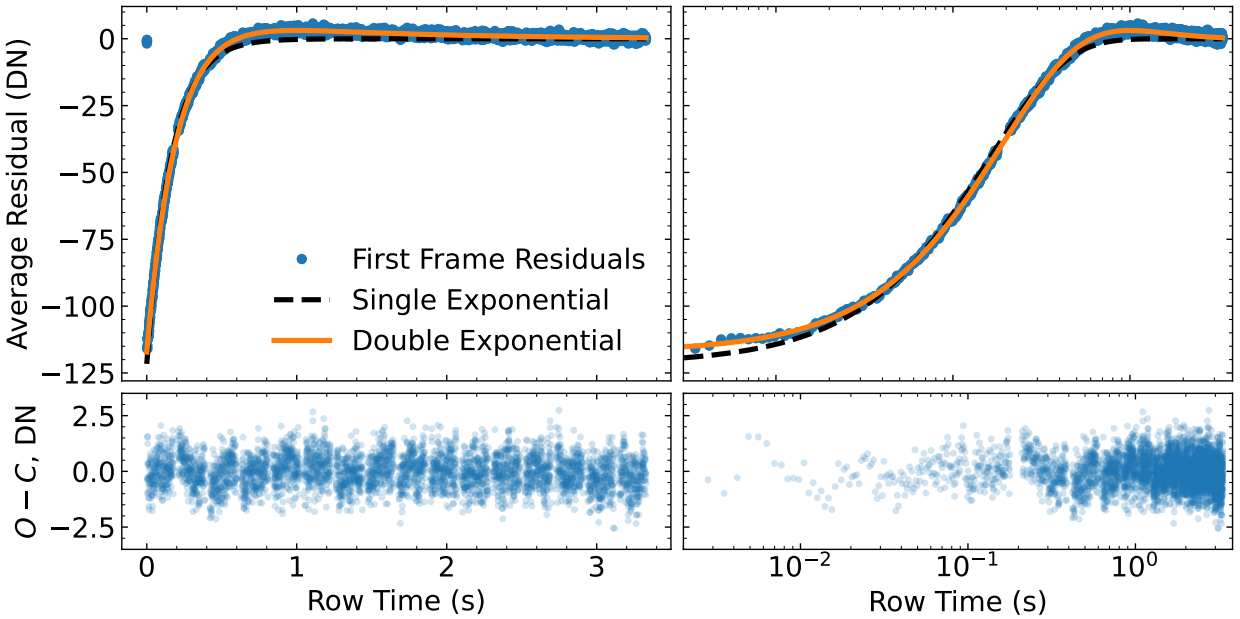

Figure 3: Best-fit sum of two exponential functions to the data shown in Figure 2. A sum of two exponentials (orange lines) provides a much better fit than a single exponential (black dashed lines), particularly at early and late times. The right panel plots the same data as the left panel, but with a logarithmic time axis. The lower panels show the residuals from the double exponential fit.

In the rest of this Technical Report, we adopt the functional form given by Equation (2) for characterizing and removing the first frame residual of detector WFI18. Charactertizations of the stability of the correction will be based on the best-fit parameters a, τ_a, b, and τ_b defined in Equation (2).

4 Temporal Variation of the Residual

We next address the temporal variation of the first-frame residual seen in Figures 1 and 2. We quantify this variation using the best-fit parameters from fitting Equation (2). We first address the short-term variation—from one exposure to the next—and then the variation as a function of temperature. For the latter we use TVAC tests taken under different instrumental conditions. The first TVAC campaign, TVAC1, was conducted in fall of 2023, while the second TVAC campaign, TVAC2, was conducted in spring of 2024. Each test campaign used a series of different temperatures for different components of the instrument: Cold Qualification (COLD_QUAL), Nominal Operations (NOM_OPS), and Hot Qualification (HOT_QUAL). For TVAC1, the data that we use was from the a phase intermediate between NOM_OPS and HOT_QUAL, designated TO_HOT_QUAL.

We first show the variation of the parameters a, b, τ_a, and τ_b (Equation (2)) over 100 exposures in the Nominal Operations phase of TVAC1. Each exposure lasted ≈3 minutes; the total length of time spanned by this data set is ≈5 hours. The detector temperature was not perfectly stable over the 100 exposures but varied by ≈0.5 K, decreasing through this

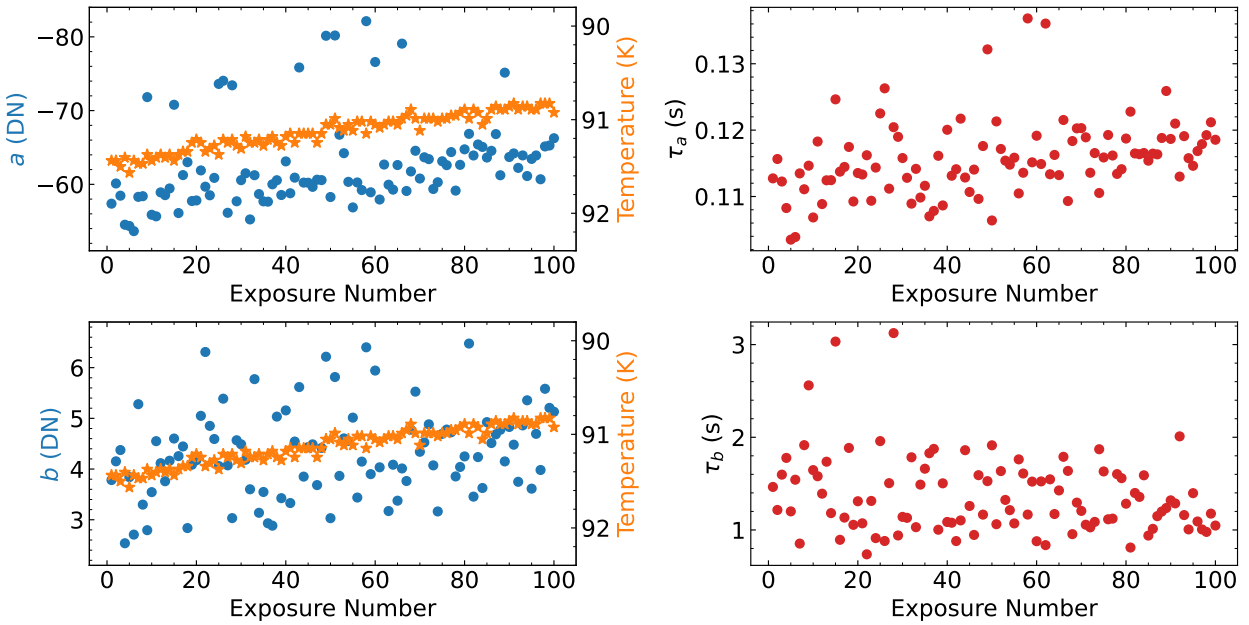

Figure 4: Best-fit parameters a, b, τ_a, and τ_b (Equation (2)) for each of a series of 100 unilluminated exposures from the Nominal Operations phase of TVAC2. The four parameters are nearly constant over this data set.

Campaign	Phase	T_{detector} K	$T_{\text{electronics}}$ K	a DN	τ_a s	b DN	τ_b s
TVAC1	COLD_QUAL	89.5	146.9	−151.5	0.211	14.5	1.02
TVAC1	NOM_OPS	91.1	152.1	−62.4	0.116	4.2	1.31
TVAC1	TO_HOT_QUAL	96.0	162.6	−17.7	0.069	1.5	2.57
TVAC2	COLD_QUAL	90.3	150.0	−124.8	0.191	10.6	1.13
TVAC2	NOM_OPS	90.3	151.9	−127.3	0.193	10.5	1.18
TVAC2	HOT_QUAL	92.8	150.6	−57.6	0.118	3.9	1.46

Table 1: Best-fit double exponential parameters.

particular test.

Figure 4 shows the time series of the four parameters of the double exponential: a, b, τ_a, and τ_b. We overplot the temperature as measured at the detector together with the best-fit coefficients a and b: the coefficients are shown with blue circles and the temperatures are shown with orange stars. The vertical axes are all ordered so that larger transient amplitudes and colder temperatures lie closer to the top of the page. For the temperature and a coefficient, this means that the vertical axes are inverted. The strengths of both exponential components of the transient appear to be anticorrelated with detector temperature during the test.

In addition to the slow changes in the amplitudes a and b of the exponentials, there are a number of one-frame fluctuations in which a suddenly increases in magnitude. Figure 4 shows twelve such upward fluctuations above the main body of points. To verify that

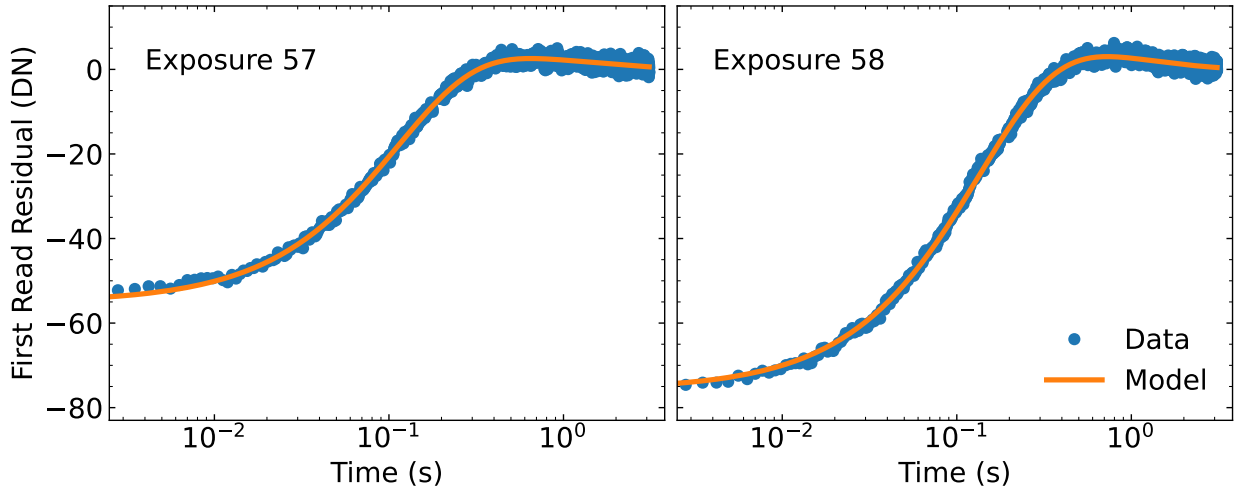

Figure 5: Change in the first-frame transient between Exposures 57 and 58 in the sequence shown in Figure 4. The single frame fluctuation is clearly visible in the row-averaged data. The functional fits are good in both frames; the sudden change in the transient is real.

these are real and do not result from a failure of the nonlinear fit, we visually compare two sequential exposures, numbered 56 and 57. These represent a point along the main body of derived values followed by the largest fluctuation of a seen in the data set. Figure 5 shows these residuals row-by-row. The double exponential model is an excellent fit to the data in both cases; the difference indicated by the fit in Figure 4 is real.

We next explore variation in different phases of TVAC, with the instrument at different thermal plateaus. We use 100 exposures at each of three temperature settings in each TVAC campaign. The actual temperatures do not necessarily match between the corresponding phases of TVAC1 and TVAC2. After performing the reference pixel correction to remove $1/f$ noise, we combine all 100 ramps into a single averaged ramp to derive characteristic values for a, b, τ_a, and τ_b. These, together with the approximate temperatures of the detector and the electronics, are listed in Table 1. All parameters show highly significant levels of variation, with the amplitudes a and b of both exponentials varying by nearly a factor of 10. The amplitudes increase with decreasing temperature, matching the trends seen in Figure 4.

Figure 6 shows the covariances between a and τ_a, and between b and τ_b. Here, we show the parameters of the average ramps (those given in Table 1) with large, outlined points, while the parameters derived from each of the 100 ramps at each TVAC phase are in smaller, semitransparent points of the same shape and color.

The left panel of Figure 6 shows the parameters of the dominant, negative exponential. The coefficient a and timescale τ_a are strongly covariant; the timescale increases with increasing amplitude. At the largest amplitudes and longest timescales, measurement precision is high. At smaller amplitudes and shorter timescales, both the strength of the signal and the number of impacted rows are smaller, making measurement error much more significant. This especially affects the blue diamonds in the lower-right corner of the left panel of Figure 6. The relationship between a and τ_a, both within and between TVAC phases, appears to be very nearly linear.

The right panel of Figure 6 shows the parameters of the longer-timescale, lower-amplitude

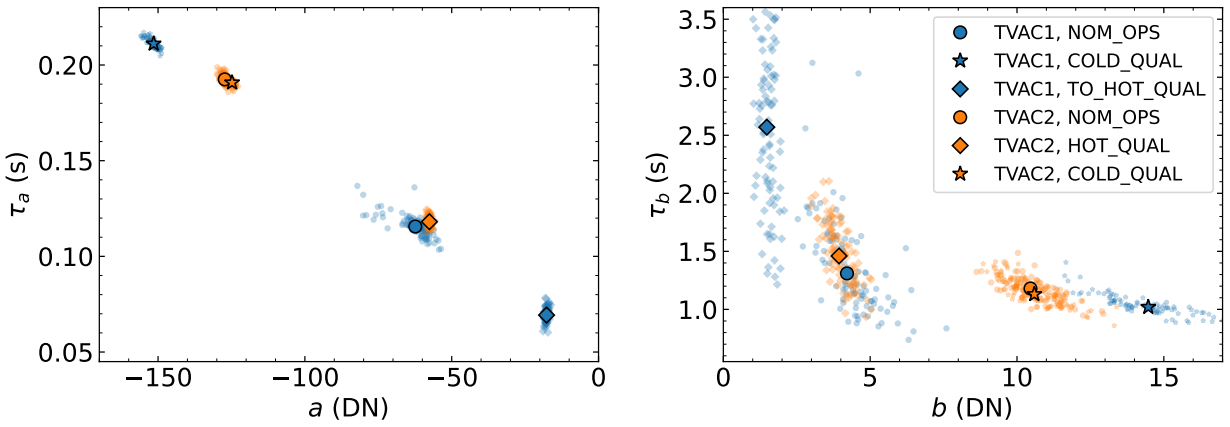

Figure 6: Covariances between the coefficients and timescales of the best-fit parameters listed in Table 1. The amplitude and time scale of the large, negative component of the first read transient are strongly coupled. Individual exposures are shown with semitransparent points. The larger points represent the transient signal fit to the average of all 100 ramps within a TVAC testing phase.

exponential. The coefficient b and timescale τ_b are again covariant, but appear to lack the linear relationship seen between a and τ_a. The covariance also goes in the opposite direction as for a and τ_a: lower amplitudes b are associated with longer exponential timescales. At lower amplitudes b, there is significant uncertainty in the measurement of both b and τ_b. At very low amplitudes of b the much longer, ∼20 second, ≈0.5 DN transient seen in all detectors by becomes relevant. In practice the stable, ≈20-s transient may be removed before fitting for the first read transient described in this report.

5 The First Read Transient on an Illuminated Exposure

The previous sections all analyzed unilluminated exposures with count rates of a few 0.01 DN/pixel/read. Flight images are expected to have sky backgrounds of a few tenths of electrons/pixel/s, or ∼1 DN/pixel/read with a readout time of ≈3 seconds and a typical gain of 2 electrons/DN. In this section we investigate the behavior and correction of the first read transient using TVAC data taken at an illumination much higher than any background level we expect to see in flight. In this way we aim to bracket the conditions of typical flight exposures.

Our illuminated data were taken in the COLD_QUAL phase of of TVAC1 with the Roman Calibration System (RCS). We use the Band 6 LED, centered at about 1750 nm, together with the F184 filter. The F184 filter has its blue edge in the middle of the Band 6 LED's spectrum. There are reflections at the filter surface at wavelengths where the filter is not transmissive. These reflections open up a scattered light path that leads to highly nonuniform illumination at the edges of Roman-WFI, including on Detector 18. The count rate in the exposure we use ranges from ≈100 DN/read to ≈1000 DN/read (≈200 to 2000

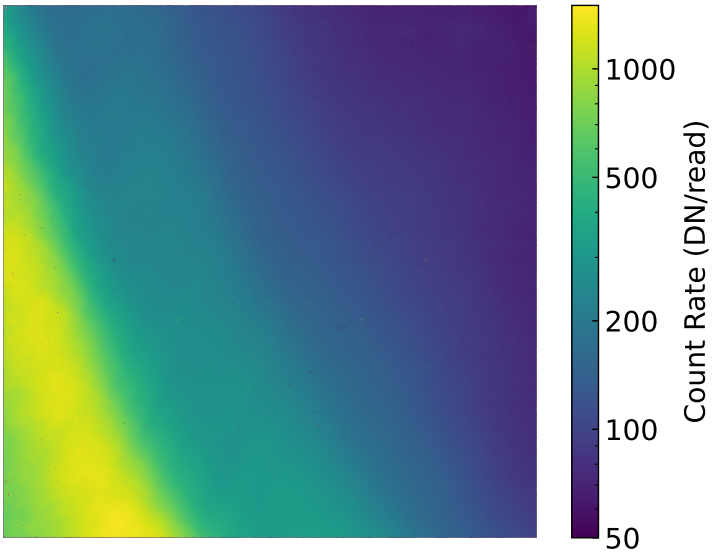

Figure 7: Count rate in units of DN/read for the illuminated exposure that we use in Section 5 (1 DN/read ≈0.6 electrons/s).

electrons/read). Figure 7 shows the count rate on this exposure in units of DN/read.

Our illuminated exposure has a sufficiently high count rate that nonlinearity cannot be ignored. To mitigate the impact of nonlinearity, we restrict our analysis to the first three reads, perform a nonlinearity correction to obtain the corrected counts y_i in read i, and compute the first frame residual as

$$y_{\rm resid} = y_1 + y_3 - 2y_2. \tag{3}$$

We then undo linearity correction to first order by inverting the quadratic approximation to nonlinearity.

The left panel of Figure 8 shows the first frame transient of the illuminated exposure shown in Figure 7. The residual is computed using Equation (3) rather than from a fit to the majority of the ramp in order to limit the impact of nonlinearity, and the averaging is restricted to pixels with a count rate below 200 DN/read. As a result, it is noisier than the residual shown in Figure 3. A double exponential remains an excellent fit to the first read even under significant illumination. The right panel of Figure 8 shows the same residual computed the same way, but for an unilluminated exposure from the same COLD_QUAL phase of TVAC1. The character of the first read transient is the same in both cases: it is nearly identical in magnitude, and is comparably well fit by the double exponential of Equation (2).

6 Removing the First Read Transient

The previous sections showed that the first read transient varies with temperature, and can suddenly change from one exposure to the next. However, it is robust to illumination of the

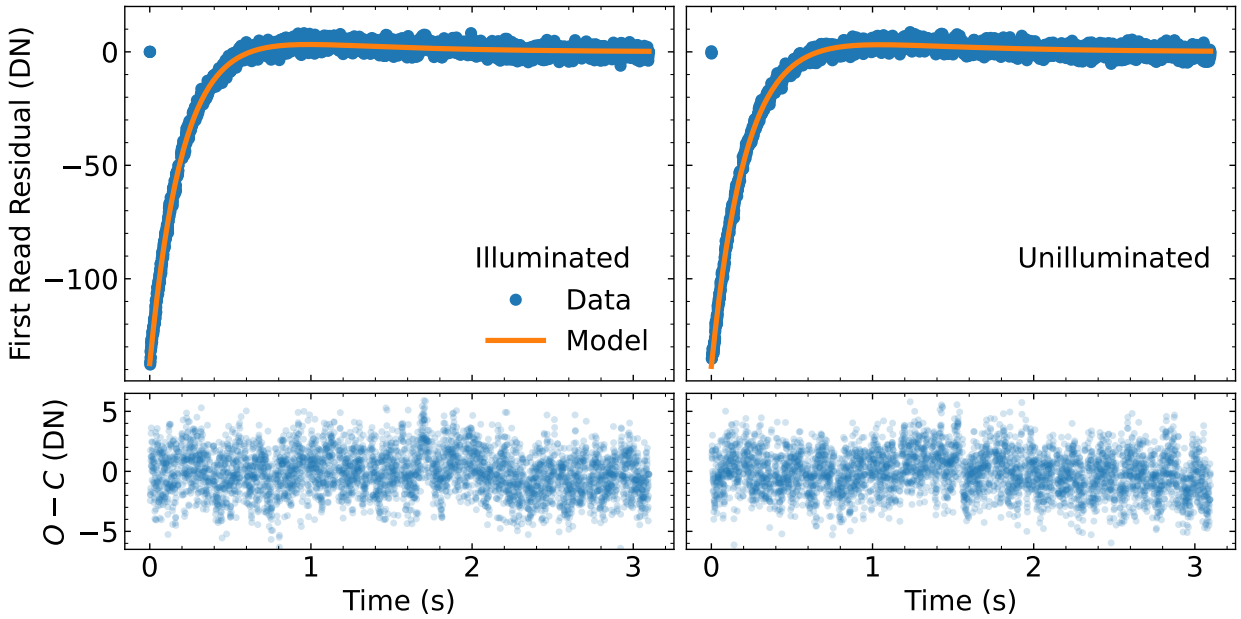

Figure 8: Left: the first read transient in the illuminated exposure shown in Figure 7; right: the first read transient in an unilluminated exposure from the same TVAC1 COLD_QUAL testing phase. Each model is fit to its own respective data points. The first read transients are nearly identical. The residuals are larger than shown in Figure 3 because we use Equation (3) rather than a least-squares fit to the majority of the ramp in order to limit the impact of nonlinearity.

detector, and it remains well-described by a double exponential in all cases. The parameters of the double exponential that describe the transient are also strongly covariant. These facts indicate that the first read transient can be removed, but they preclude the use of a static correction given in a reference file. Instead, we must fit for the transient separately in each exposure.

Our characterization in this Technical Report began with the suppression of $1/f$ noise using the Improved Roman Reference Correction. This correction will be applied to all Roman-WFI data as a first step, before computing the first frame residual. We expect that the ≈20-s-long transient identified by Betti et al. (2025) will also be removed. After this step, we suggest the following procedure:

1. Fit a slope and reset value to the ramp excluding the first read and possibly excluding the second read. This slope may be fit using fixed weights that are optimal in the read noise limit, and may be limited to a small number of reads. In the simplest case, the slope may be estimated from the difference between the second and third resultants.

2. Compute the first read residual from the prediction based on this slope and reset value.

3. Construct a mask of pixels with low illumination to be used for fitting the first read transient.

4. Compute the row-by-row sigma-clipped mean on the low illumination pixels.

5. Use a nonlinear optimization routine like `scipy.optimize.curve_fit` to fit for the parameters. For this step, guesses for the parameters, informed by the results from this Technical Report, will need to be supplied.

6. Use the actual timing pattern for all pixels to apply the correction.

The procedure above matches the approach that we used in the earlier sections. For the unilluminated exposures, we used all reads from the third read onwards to determine the slope and offset of the ramp. For the illuminated exposure analyzed in Section 5, we used only the second and third reads. We also must provide initial guesses for the values of all parameters. For the analyses earlier in this report, we initialize a to the 1.1 times value of the residual at the first row, b to $-a/11$, τ_a to 0.2 seconds, and τ_b to 1 second. These starting values will need to be monitored throughout Roman flight operations, with the subdominant exponential much more vulnerable to being fit incorrectly.

The algorithm proposed above will fail if all pixels are highly illuminated. This will occur when taking high-illumination flat fields and when performing some lamp on-lamp off (LOLO) tests for linearity. In those cases it will still be possible to compute the first frame residual, but it will require a more careful treatment of nonlinearity. To avoid an explicit failure a minimum fraction (e.g. 50%) of the pixels in each row could be used, with the quality of the correction suffering somewhat at high illuminations. The procedure above also does not allow for the case of the first read being averaged together with other reads to form the first resultant. All currently-planned readout patterns for Roman-WFI keep the first read as its own resultant. In practice, little of the first read transient remains in the second read, so it can probably still be removed by this approach even if the first resultant comprises more than one read.

The computational cost of the algorithm proposed here will be lower than the cost of fitting a ramp using optimal weights, as it will only require a single, simple summation of resultants to estimate the count rate. A row-by-row sigma-clipped mean only needs to be computed for a single resultant, limiting the impact of this step. The nonlinear optimization only fits to 4096 rows and will therefore be fast.

7 Conclusions

In this Technical Report, we have quantified a transient signal seen in the first read of detector 18 on Roman-WFI. We have shown that it is well-fit by the sum of two exponentials, but that the parameters describing this function are strongly covariant with one another, vary with temperature, and can fluctuate from one exposure to the next. While the first read transient varies, it is accurately described by our adopted functional form in all exposures we have investigated, at a range of temperatures and illuminations.

After demonstrating both the uniformity of the functional form of the first read anomaly and the wide range of variations of its magnitude and time constants, we propose an algorithm to fit and remove it from science data. The details of this algorithm will need to be tested for robustness on flight data, with the quality of the correction monitored throughout the Roman mission.

References

Betti, S., Brandt, T., Casertano, S., et al. 2025, The Statistical Properties of Dark Ramps for the Roman-WFI Detectors, Tech. Rep. Technical Report Roman-STScI-000814, STScI

Betti, S. K., Casertano, S., Brandt, T., et al. 2024, Application and Characterization of IRRC on Roman/WFI TVAC1 Data, Nancy Grace Roman Space Telescope Technical Reports, 16 pp., ,

Domber, J. L., Gygax, J. D., Aumiller, P., et al. 2022, in Society of Photo-Optical Instrumentation Engineers (SPIE) Conference Series, Vol. 12180, Space Telescopes and Instrumentation 2022: Optical, Infrared, and Millimeter Wave, ed. L. E. Coyle, S. Matsuura, & M. D. Perrin, 121801O

Rauscher, B. J. 2015, PASP, 127, 1144

Rauscher, B. J., Fox, O., Ferruit, P., et al. 2007, PASP, 119, 768

Schlieder, J. E., Barclay, T., Barnes, A., et al. 2024, in Society of Photo-Optical Instrumentation Engineers (SPIE) Conference Series, Vol. 13092, Space Telescopes and Instrumentation 2024: Optical, Infrared, and Millimeter Wave, ed. L. E. Coyle, S. Matsuura, & M. D. Perrin, 130920S